Electronic Supplementary Material (ESI) for ChemComm.

Supporting information

Tuning the electronic state of metal/graphene catalysts for the control of catalytic activity via N- and B-doping into graphenes

*Yang Sik Yun,[a,†] Hongseok Park,[a,†] Danim Yun,[a] Chyan Kyung Song,[a] Tae Yong Kim,[a] Kyung Rok Lee,[a] Younhwa Kim,[a] Jeong Woo Han,[b] and Jongheop Yi[a,]**

[a] World Class University Program of Chemical Convergence for Energy & Environment, School of Chemical and Biological Engineering, Institute of Chemical Processes, Seoul National University, Seoul 151-742, Republic of Korea

[b] Department of Chemical Engineering, Pohang University of Science and Technology, Pohang 37673, Republic of Korea

[†] These authors contributed equally to this work.

*To whom correspondence should be addressed: jyi@snu.ac.kr

Tel: +82 2-880-7438

CONTENTS

Experimental and computational details

1. Preparation of the catalysts

Graphene oxide (GO) was prepared via following a procedure reported in a previous study.[S1] H_2SO_4 (180 mL, ≥95%, Samchun) and H_3PO_4 (20 mL, ≥85%, Samchun) were mixed. And then, 1.5 g of graphite (Sigma-aldrich) was added to the mixture. 9.0 g of $KMnO_4$ (99%, Sigma-aldrich) was then slowly added with vigorous stirring for 12 h at 40 °C. The mixture was cooled down to ambient temperature, and 200 mL of an aqueous H_2O_2 solution (190 mL of deionized water + 10 mL of 30 wt.% in H_2O_2) was then added. The solution stirred for 1 h. The precipitate was then washed with deionized water, HCl (35-37%, Samchun), and ethanol repeatedly. The washed precipitate was coagulated with ether (≥99%, Sigma–Aldrich). Finally, yellow powder was obtained by vacuum-drying overnight at room temperature.

For the preparation of N-doped graphene (N-G), 2 g of GO was heated under an ammonia atmosphere at three different temperatures (700, 800, and 900 °C) for 4 h. The as-obtained samples were denoted as N-G(700), N-G(800), and N-G(900). B-doped graphene (B-G) was synthesized by annealing 2 g of GO powder with mixed with excess boric acid under a N_2 atmosphere at different temperatures (700, 800, and 900 °C) for 4 h. The samples were denoted as B-G(700), B-G(800), and B-G(900). Undoped graphene (un-G) was prepared by annealing 2 g of GO powder under a N_2 atmosphere at 500 °C for 4 h.

3 wt.% cobalt on N-G, un-G, and B-G (Co/N-G, Co/un-G, and Co/B-G) was prepared by following procedure. A 0.3 g of support (N-G, un-G, and B-G) was dispersed in an admixture of 15 mL of ethanol (≥99.5, Sigma-Aldrich) and 15 mL of deionized water, which was then sonicated for 1 h. Then, 1mL of aqueous solution containing the calculated amount of cobalt nitrate hexahydrate (99.999%, Sigma-Aldrich) was added to the support dispersed solution.

The solution was further sonicated for 1 h. The solvent was then removed by evaporation under reduced pressure at room temperature, and the resulting solids were dried overnight at 85 °C. The samples were reduced under 10 vol.% H_2/He flow at 550 °C for 3 h. Cube-shaped palladium nanoparticles were synthesized according to a previously described method.[S2] Palladium supported on N-G(700), un-G, and B-G(700) were prepared by incipient wetness method. The samples were denoted as Pd/N-G(700), Pd/un-G, and Pd/B-G(700).

2. Characterization

XRD analysis was performed by Rigaku d-MAX2500-PC (Cu Kα radiation, 50 kV, 100 mA). JEOL JEM-3010 microscope was operated to obtain high-resolution transmission electron micrograph (HR-TEM) images at 300 kV of an acceleration voltage. The BET hysteresis of each catalyst was obtained at -196 °C using a Micrometrics ASAP-2010 system. The corresponding surface area was measured by the BET method (P/P_0=0.05~0.15). Raman spectra were recorded using a HORIBA T64000 (a multichannel CCD detector, Ar laser at 514 nm) at ambient temperature. The loading amount of active metal on support was analyzed by inductively coupled plasma atomic emission spectroscopy (ICP-AES, OPTIMA 4300DV). X-ray photoelectron spectroscopy (XPS) spectra were obtained by a AXIS-His (KRATOS). The binding energies of each Co 2p, Pd 3d, N 1s, and B 1s were referenced to the C 1s at 284.5 eV.

3. Catalytic activity test

The catalytic activity test for CO hydrogenation was carried out at 450 ^oC under atmospheric pressure. A powder sample (0.1 g) was loaded in a reactor (11 mm i.d., quartz). The catalyst was preheated to the reaction temperature under a reducing atmosphere (H_2 and N_2) at 450 °C for 1 h before the reaction. Total flow was fixed at 41 mL/min. The molar ratio

of H_2 to CO was 2. N_2 (3 mL/min) and He (29 mL/min) were used as an internal standard and a carrier, respectively.

For the reaction kinetic studies, the partial pressures of CO and H_2 (P_{CO} and P_{H2}, respectively) were controlled, and Ar was used to balance the total flow (30 mL/min). N_2 (3 mL/min) was injected as an internal standard. The reaction tests were conducted over 0.05 g of catalyst at temperature range of 400-450 ^oC. In each test, CH_4 and H_2O were produced due to low reaction pressure (1 atm).

For 4-nitrophenol (4-NP) reduction, 0.1 mg of catalyst was added to an aqueous solution of 5.618 mM of $NaBH_4$ and 0.112 mM of 4-NP at room temperature. The time dependent reduction was elucidated from the absorbance spectra by using a Jasco V670 spectrometer.

4. Computational details

For the density functional theory (DFT) calculations, the Vienna Ab-initio Simulation Package (VASP) was used.[S3] The exchange-correlation energy of electrons was treated with the generalized gradient approximation (GGA) parameterized by the Perdew-Burke-Ernzerhof (PBE).[S4] The electron-ion interactions were described by the projector augmented wave (PAW) method.[S5] All calculations include DFT-D2 Grimme's empirical correction.[S6] For the bulk optimization of graphene (N-G, un-G, and B-G), a plane-wave basis set with an cutoff of 520 eV was used. A Monkhorst-Pack mesh of 9 × 9 × 1 in the Brillouin zone was used for the bulk optimizations. For the other calculations, the Brillouin zone was sampled using a Monkhorst−Pack mesh of 5 × 5 × 1 k-points with an energy cutoff of 400 eV. The convergence criteria were for ionic optimization steps (0.03 eV/Å) and self-consistent iterations (2×10^{-4} eV), respectively. A Methfessel−Paxton smearing of 0.2 eV and a Gaussian smearing of 0.01 eV were used for the optimized N-G, un-G, and B-G models, and

Co/N-G, Co/un-G, and Co/B-G, respectively. Bader charge analysis was used to investigate the electron transfer phenomena.[S7]

Charge variation in the atoms of molecule or slab was calculated as

$$\Delta q = q_{\text{non-interacting}} - q_{\text{interacting}}$$

where $q_{\text{non-interacting}}$ is the charge of the atom in non-interacting system (the bare slab or the molecule in the gas phase), and $q_{\text{interacting}}$ is the charge of the atom in the system at which the molecule is adsorbed on the slab. In this convention, negative value indicates a gain of electron. Fermi-level was also obtained in charge calculations.

As model systems, Co/N-G, Co/un-G, Co/B-G models were developed based on several assumptions and experimental results. For the modeling, we assumed that N-G, un-G, and B-G were clean single-layered surfaces without defects and surface oxygen-containing groups, the dopant species were homogeneously distributed in the developing models, and the shape of Co nanoparticle on N-G, un-G, B-G was hemisphere. Graphene (un-G) was constructed by an single-layer with p(5×3) rectangular unit cell (12.34 Å × 12.83 Å). On the basis of un-G model, N-G was modeled by replacing C atom with N atom (~1.66 at.%). According to XPS results (Fig. 1A and Table S2), a fraction of pyridinic and pyrrolic N (p-type) was decreased while that of quaternary N (n-type) was increased as the annealing temperature was increased.[S8,S9] In addition, quaternary N has a strong effect on electronic state compared to other ones.[S9,S10] These indicate that the effect of quaternary N species on electronic state could be dominant rather than that of other N structures in the this system. Thus, quaternary N was determined as a doping structure of N atom in N-G model. For the comparison, the counterpart (B-G) was also developed in the similar manner to N-G. The models were shown in Fig. S5.

Co clusters was constructed considering the experimental results that peak corresponding to metallic FCC Co was observed in XRD patterns of Co/N-G, Co/un-G, and Co/B-G samples. Co_{10} cluster was chosen as a model cluster to represent hemisphere Co nanoparticle deposited on N-G, un-G, and B-G.[S11] For the determination of most stable configuration of Co/N-G, Co/un-G, and Co/B-G models, various adsorption sites of Co cluster on N-G, un-G, and B-G were screened. Finally, we used them as model systems to compare adsorption behaviors of CO and H molecules on Co supported on N-G, un-G, and B-G.

Kinetic study

Although controversies remain concerning the CO dissociation pathway, it was demonstrated that the CO dissociation on cobalt nanoparticle is assisted by hydrogen.[S8] The Langmuir-Hinshelwood (LH) rate expression for CO conversion is derived the assumption of CO dissociation pathway assisted by hydrogen. The steps of hydrogen assisted CO dissociation pathway are below.

$$H_2 + 2* \overset{K_{H_2}}{\leftrightarrow} 2H* \quad \text{(S1)}$$

$$CO + * \overset{K_{CO}}{\leftrightarrow} CO* \quad \text{(S2)}$$

$$CO* + H* \overset{K_1}{\leftrightarrow} HCO* + * \quad \text{(S3)}$$

$$HCO* + H* \overset{k_2}{\rightarrow} HCOH* + * \quad \text{(S4)}$$

$$HCOH* + * \overset{k_3}{\rightarrow} CH* + OH* \quad \text{(S5)}$$

$$OH* + H* \leftrightarrow H_2O + 2* \quad \text{(S6)}$$

Assume that steps 1 to 3 are quasi-equilibrium and step 4 is considered as a rate determining step for CO conversion.[S12]

$$\theta_H = \sqrt{K_{H_2} P_{H_2}}\,\theta_*$$

$$\theta_{CO} = K_{CO} P_{CO} \theta_*$$

Pseudo steady-state for HCO* species

$$k_1\theta_{CO}\theta_H - k_{-1}\theta_{HCO}\theta_* = 0$$

$$\theta_{HCO} = K_1 K_{CO} P_{CO} \sqrt{K_{H_2} P_{H_2}}\,\theta_*$$

$$-r_{CO} = k_2\theta_{HCO}\theta_H = k_2 K_1 K_{CO} K_{H_2} P_{CO} P_{H_2}\theta_*^{\,2}$$

$$\theta_* + \theta_{CO} + \theta_H + \theta_{HCO} = 1$$

$$\theta_* = \frac{1}{1 + K_{CO}P_{CO} + \sqrt{K_{H_2}P_{H_2}} + K_1 K_{CO} P_{CO}\sqrt{K_{H_2}P_{H_2}}}$$

Assume that CO* and * are the most abundant reaction intermediate based on the results in Fig. S. The high coverage of adsorbed CO molecules on the surface is considered to hinder the conversion of CO. Therefore, the above expression can be simplified as below.

$$\theta_* = \frac{1}{1 + K_{CO}P_{CO}}$$

$$-r_{CO} = k_2\theta_{HCOH}\theta_* = \frac{k_2 K_1 K_{H_2} K_{CO} P_{CO} P_{H_2}}{(1 + K_{CO}P_{CO})^2}$$

$$-r_{CO} = \frac{k_{app} K_{CO} P_{CO} P_{H_2}}{(1 + K_{CO}P_{CO})^2} \qquad \text{(Equation S1)}$$

where $-r_{CO}$ is the rate of CO conversion, P_{CO} is the CO partial pressure, P_{H_2} is the H_2 partial pressure, and the parameters k_{app} and K_{CO} represent an apparent rate constant and the CO adsorption constant, respectively.

- **Figures**

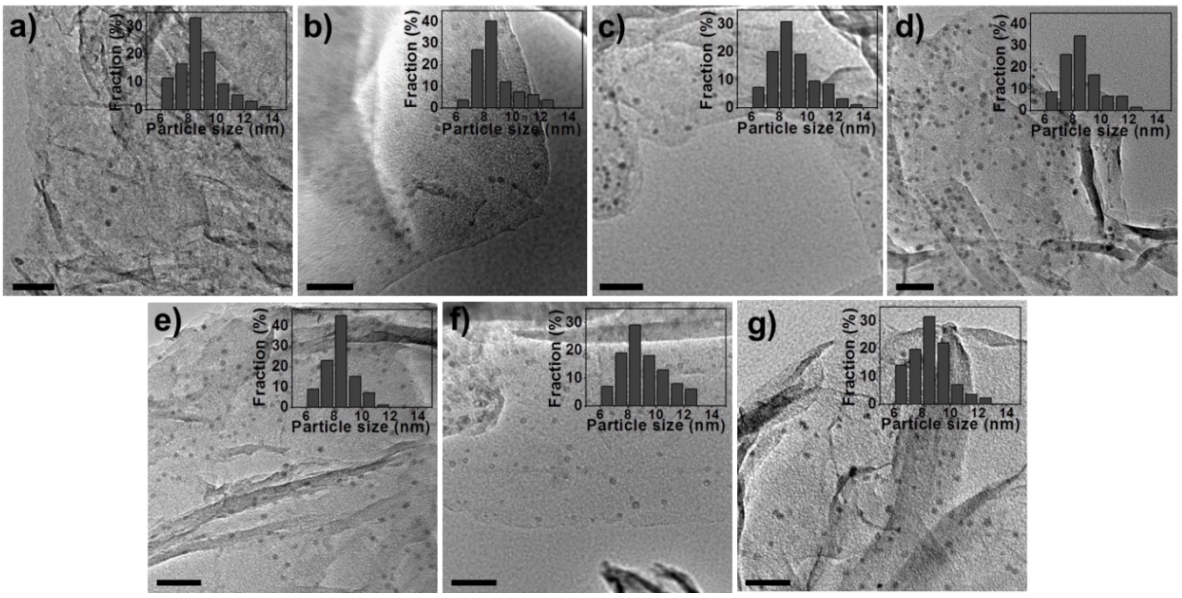

Fig. S1. TEM images of a) Co/N-G(900), b) Co/N-G(800), c) Co/N-G(700), d) Co/un-G, e) Co/B-G(700), f) Co/B-G(800), and g) Co/B-G(900). Each Scale bar represents 50 nm.

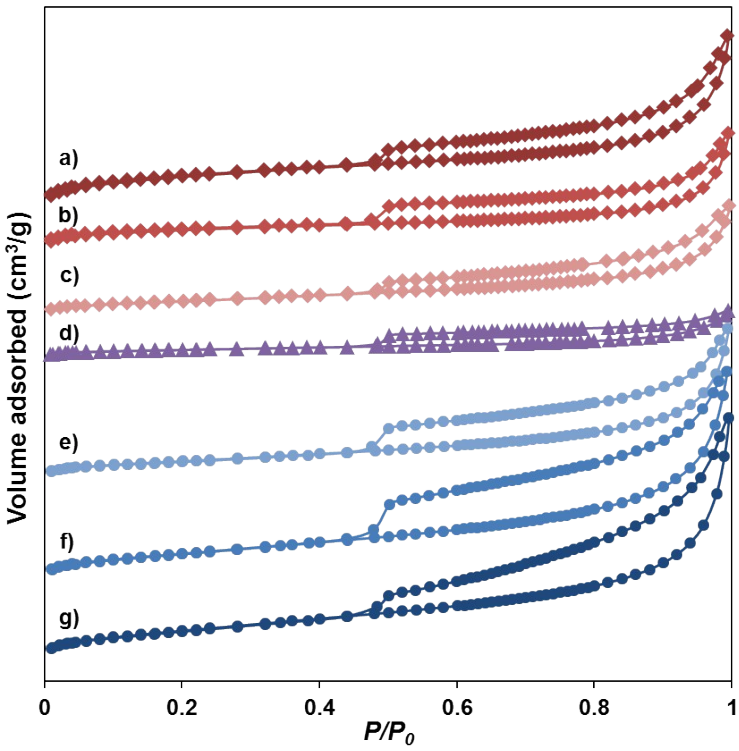

Fig. S2. N_2 adsorption-desorption isotherms of a) Co/N-G(900), b) Co/N-G(800), c) Co/N-G(700), d) Co/un-G, e) Co/B-G(700), f) Co/B-G(800), and g) Co/B-G(900).

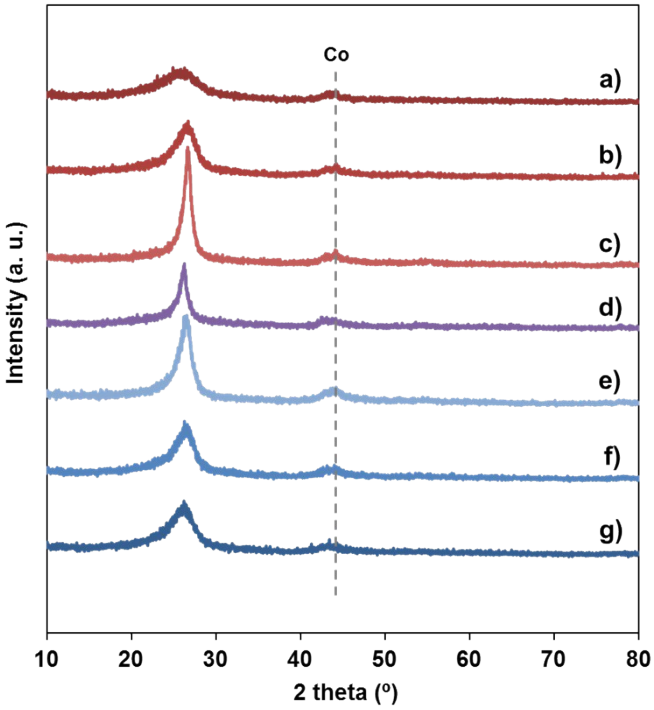

Fig. S3. XRD patterns of a) Co/N-G(900), b) Co/N-G(800), c) Co/N-G(700), d) Co/un-G, e) Co/B-G(700), f) Co/B-G(800), and g) Co/B-G(900).

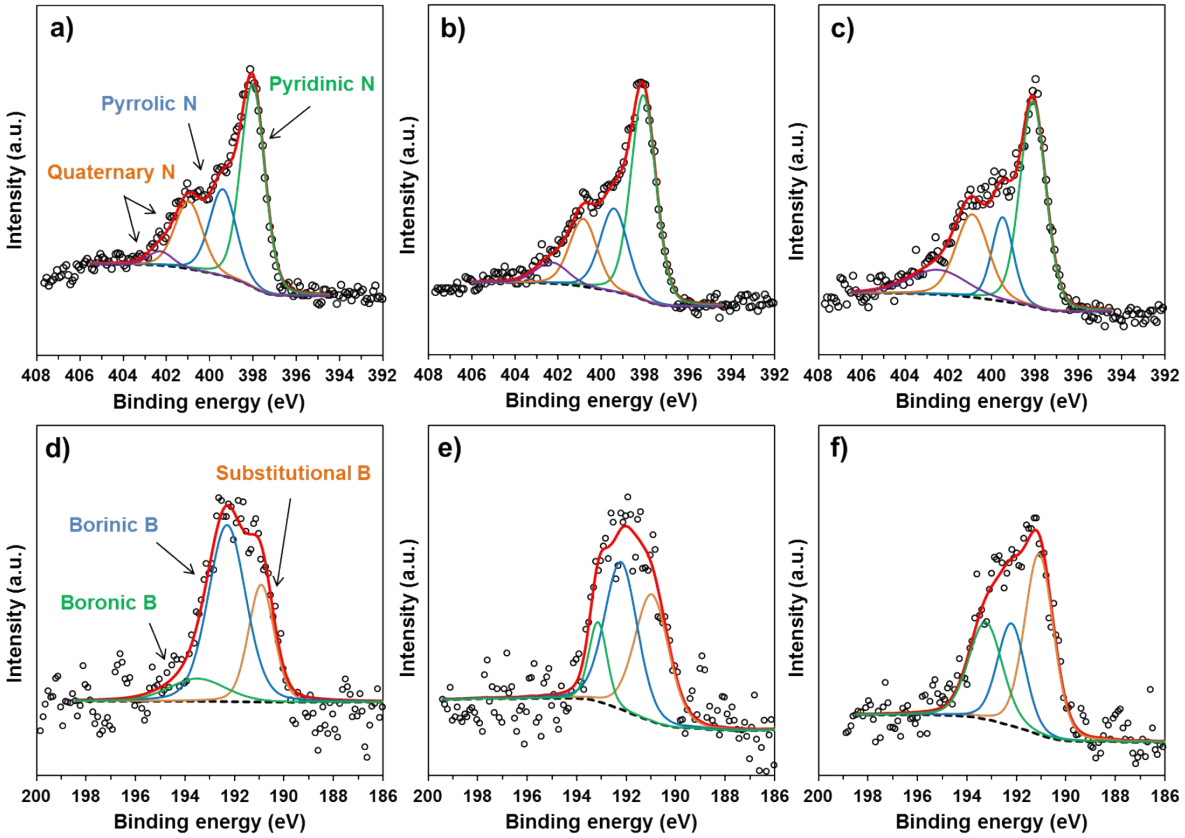

Fig. S4. XPS spectra of N 1s for a) Co/N-G(700), b) Co/N-G(800), and c) Co/N-G(900), and B1s for d) Co/B-G(700), e) Co/B-G(800), and f) Co/B-G(900). N1s spectra were deconvoluted into the four types of nitrogen, which includs pyridinic (398.1 eV), pyrrolic (399.5 eV), quaternary center (400.9 eV) and quaternary valley (402.5 eV).[S13] The B1s peak for Co/BG includes three different doping states of boron within graphene: substitutional (190.9 eV), borinic (192.3 eV), and boronic (193.2 eV).[S14]

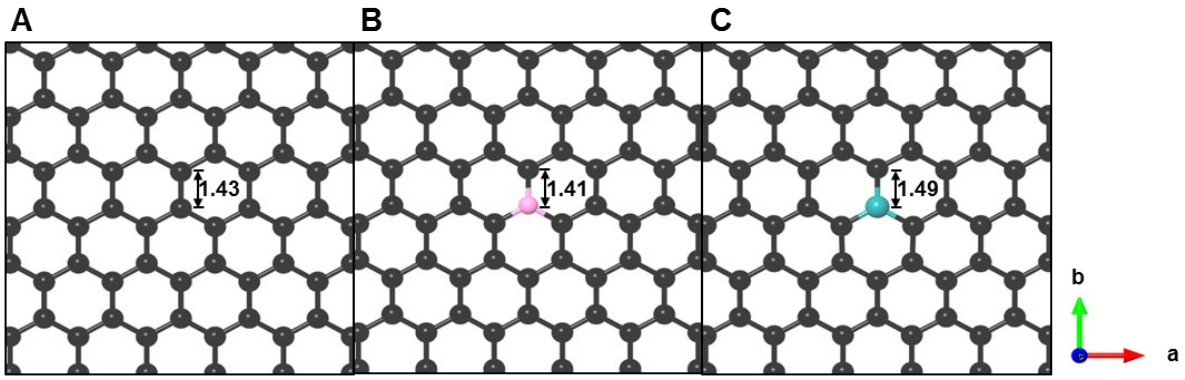

Fig. S5. Calculation models of A) un-G, B) N-G, and C) B-G. Black, pink, and green spheres correspond to C, N, and B atoms, respectively. The distances are in Å.

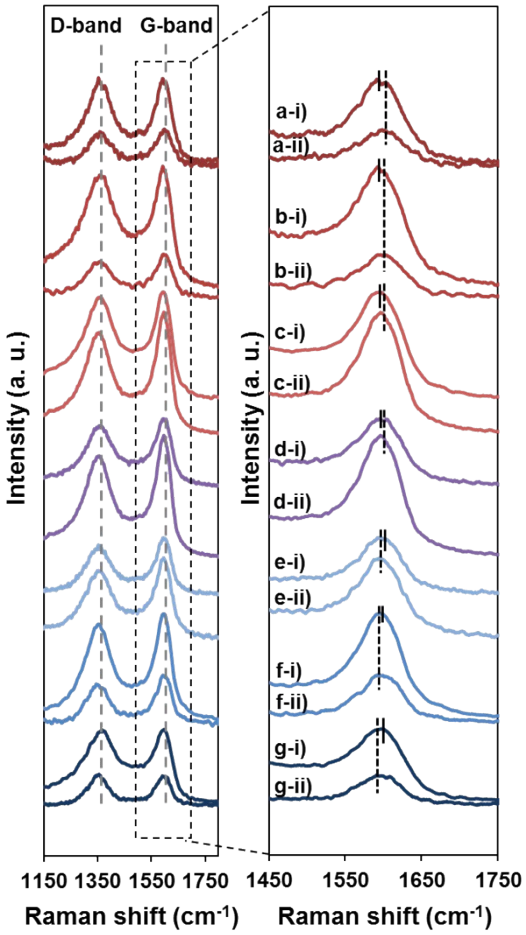

Fig. S6. Raman shift i) before and ii) after Co was loaded on supports: a) N-G(900), b) N-G(800), c) N-G(700), d) un-G, e) B-G(700), f) B-G(800), and g) B-G(900). Solid and dotted line in right figure represents the peak of G-band before and after Co was loaded on supports, respectively.

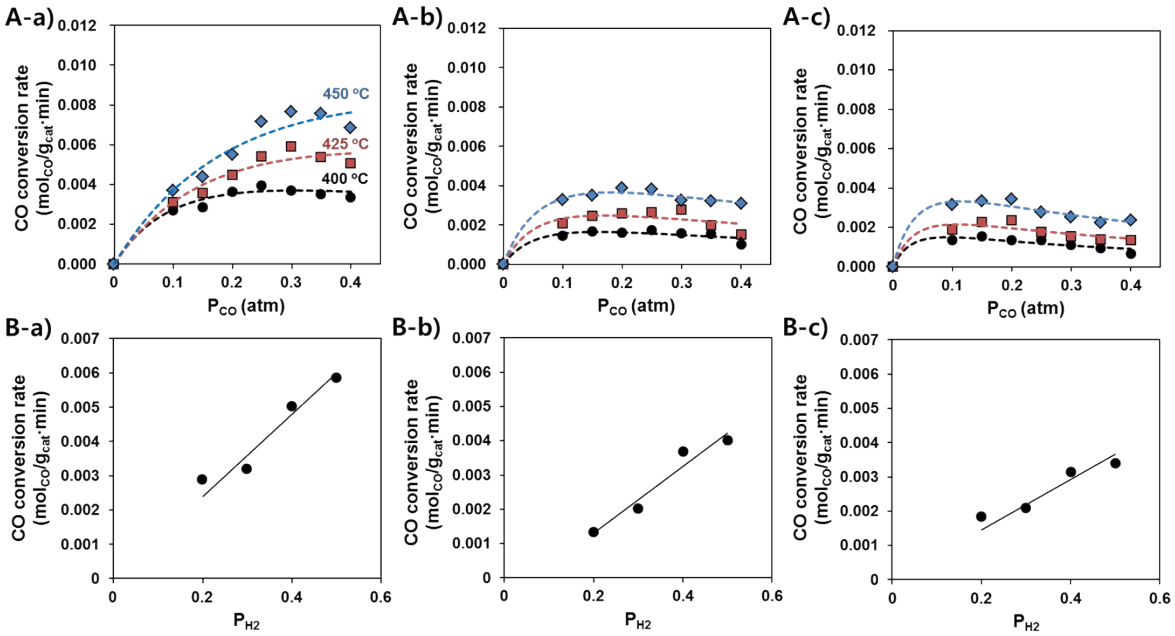

Fig. S7. The rate of CO conversion over a) Co/N-G(900), b) Co/un-G, and c) Co/B-G(700) as a function of A) P_{CO} (P_{H2} = 0.4 atm) at 400-450 °C, and B) P_{H2} (P_{CO} = 0.2 atm) at 450 °C. The curves in the plots correspond to the model equation.

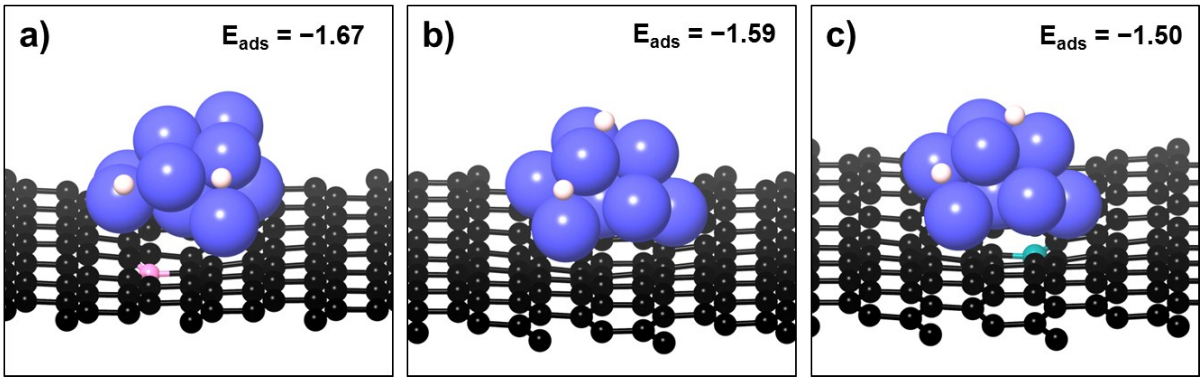

Fig. S8. The most stable adsorption structure of two H atoms on a) Co/N-G, b) Co/un-G, and c) Co/B-G models. Black, pink, green, violet-blue, and white spheres correspond to C, N, B, Co, and H atoms, respectively. The E_{ads} indicates the adsorption energy of the two H atoms on Co cluster (E_{ads}= $E_{Co/support+2H(ads)}$ − $E_{Co/support}$ − $E_{H2(molecule)}$).

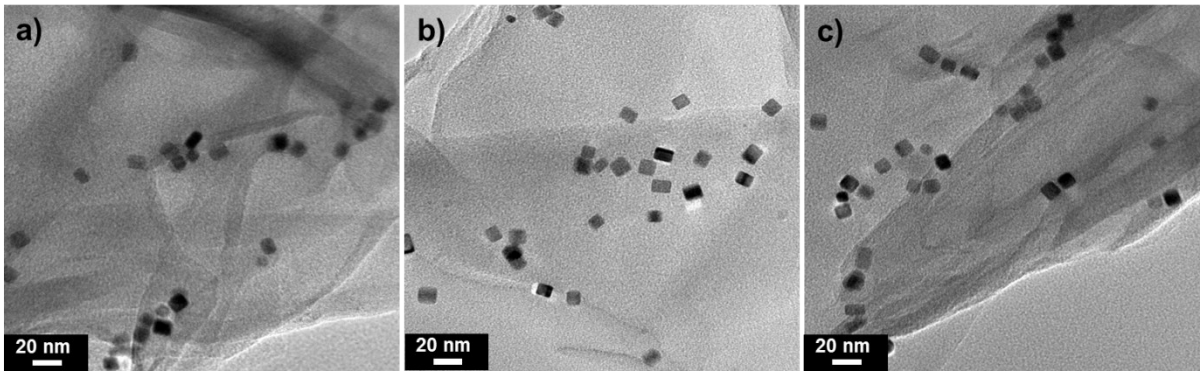

Fig. S9. TEM images of a) Pd/N-G(700), b) Pd/un-G, and c) Pd/B-G(700).

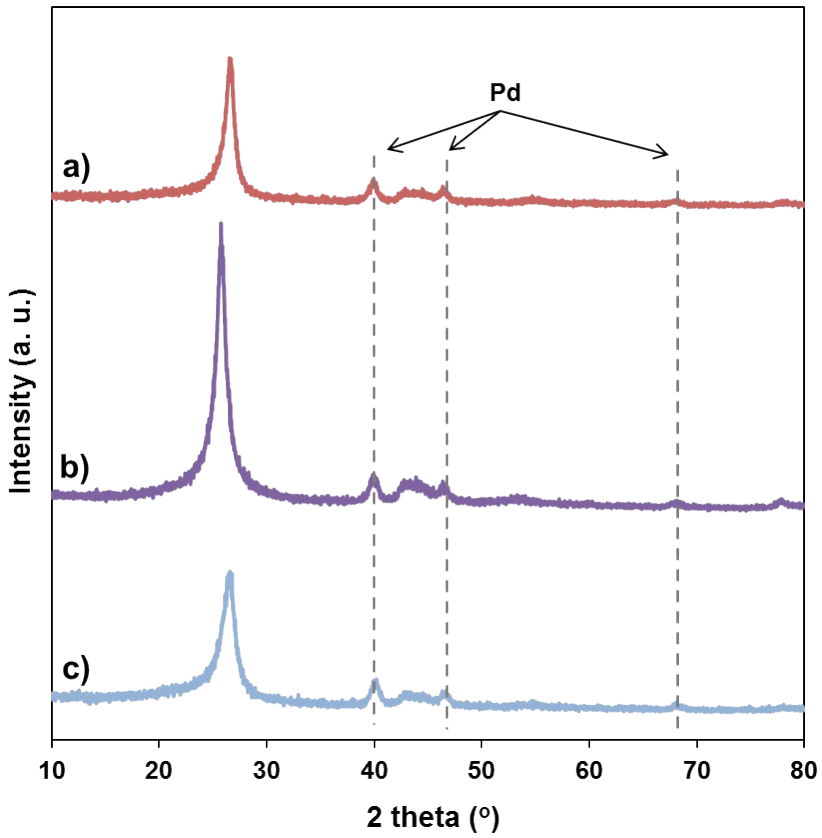

Fig. S10. XRD patterns of a) Pd/N-G(700), b) Pd/un-G, and c) Pd/B-G(700)

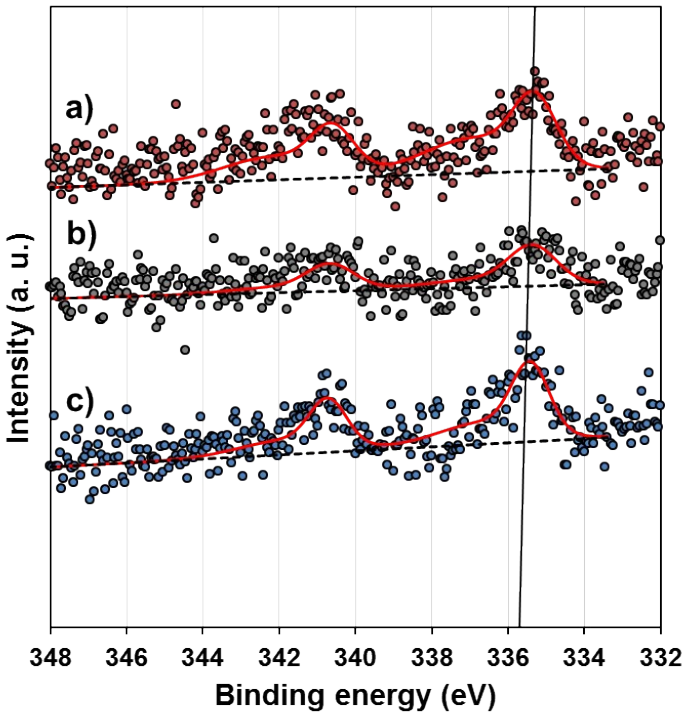

Fig. S11. XPS spectra of Pd 3d for a) Pd/N-G(700), b) Pd/un-G, and c) Pd/B-G(700).

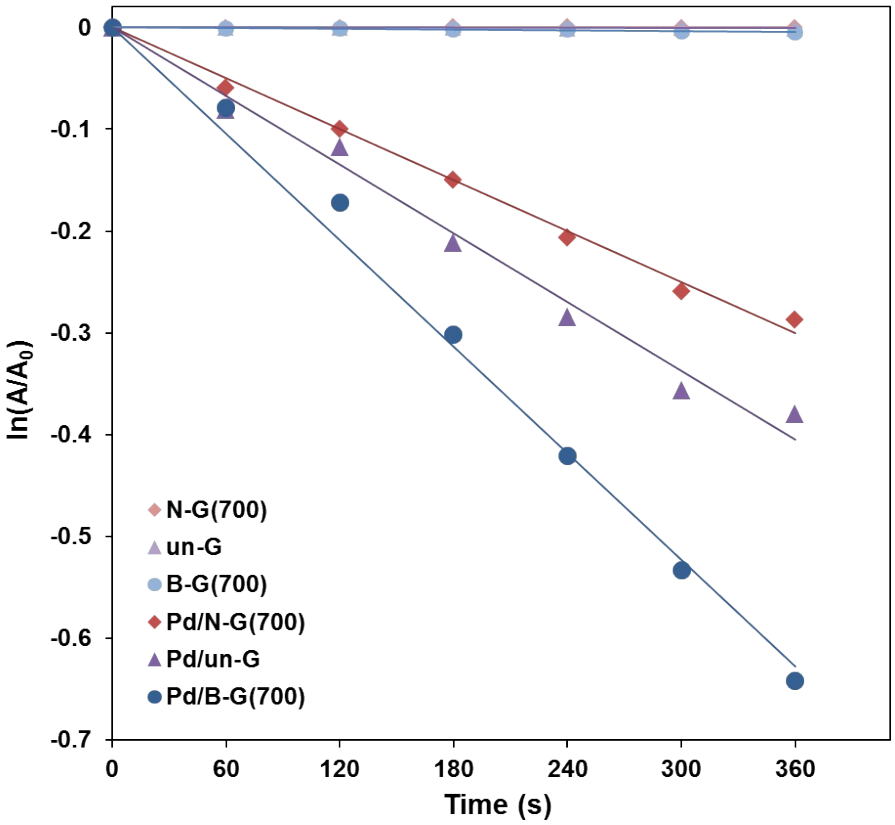

Fig. S12. Plot of ln(A/A0) versus time for the 4-nitrophenol reduction over N-G(700), un-G, B-G(700), Pd/N-G(700), Pd/un-G, and Pd/B-G(700). Reaction condition: 0.1 mg of catalyst, 5.6 mM of $NaBH_4$, 0.112 mM of 4-nitrophenol, and 25 ^oC.

It is widely accepted that the reduction of 4-NP by $NaBH_4$ follows Langmuir-Hinshelwood mechanism.[S15] In the condition that concentration of $NaBH_4$ is in excess compared to that of 4-NP, the reaction rate depends on adsorption of 4-NP. [S16,S17] In this work, about 50 times higher concentration of $NaBH_4$ was used than that of 4-NP. Thus, adsorption of 4-NP is an important and determining step for the reaction rate in our condition. In solution, 4-NP forms 4-nitrophenolate via deprotonation in the presence of $NaBH_4$, and it exhibited negative charge (Scheme S1).[21] In addition, 4-nitrophenolate is adsorbed on the metal surface via partially negatively charged oxygen functional group in NO_2 group.[S18] Consequently, electrostatic interactions between the reactant and metal have largely influence on the 4-NP adsorption, and corresponding activity. In this study, the electron density of Pd were ordered as Pd/N-G(700) > Pd/un-G > Pd/B-G(700) in Fig. S11. Based on the reaction mechanism, 4-NP (or 4-nitrophenolate) can be preferentially adsorbed on relatively more electrophilic Pd on B-G compared to the others, leading to high activity.

● Tables

Table S1. Physicochemical properties of the prepared Co/N-G, Co/un-G, and Co/B-G samples.

	D_{ave}[a]	N content[b] (at.%)	B content[b] (at.%)	Co content[c] (wt.%)	BET surface area[d] (m^2/g)	Pore volume[e] (cm^3/g)
Co/N-G(900)	8.6	4.31	-	3.26	371.3	0.402
Co/N-G(800)	9.0	5.77	-	2.97	305.2	0.265
Co/N-G(700)	8.4	5.97	-	2.96	127.7	0.241
Co/un-G	8.6	-	-	3.27	74.5	0.106
Co/B-G(700)	9.0	-	1.05	3.28	152.8	0.329
Co/B-G(800)	8.8	-	0.94	3.23	248.0	0.464
Co/B-G(900)	8.7	-	1.49	3.04	239.8	0.534

[a]D_{ave} indicates average sizes of Co nanoparticle on N-G, un-G, and B-G samples, measured based on each TEM image.

[b]N and B contents in the catalysts were measured by XPS analysis.

[c]Loading weight percent of Co was analyzed by ICP analysis.

[d]The Brunauer–Emmett–Teller (BET) surface area was determined from the N_2 adsorption branch in the relative pressure range from 0.05 to 0.12.

[e]Total pore volume (V_{total}) was evaluated at a relative pressure of 0.99.

Table S2. The amounts (at.%) of pyridinic, pyrrolic, and quaternary N in Co/N-G samples, and borinic, boronic, and substitutional B in Co/B-G samples.[a]

	Pyridinic N	Pyrrolic N	Quaternary N
Co/N-G(700)	3.45	1.63	1.56
Co/N-G(800)	3.29	1.47	1.63
Co/N-G(900)	2.39	0.65	1.81
	Borinic B	Boronic B	Substitutional B
Co/B-G(700)	0.56	0.11	0.25
Co/B-G(800)	0.37	0.11	0.34
Co/B-G(900)	0.33	0.37	0.60

[a]The compositions of N and B were determined by XPS.

Table S3. DFT-calculated Fermi levels of N-G, un-G, and B-G models.

	N-G	un-G	B-G
Fermi level (eV)	-2.50	-3.17	-3.66

Table S4. G-bands of N-G, un-G, B-G, Co/N-G, Co/un-G, and Co/B-G at different annealing temperatures, and the corresponding differences (Δ) between supports and catalysts.

Catalyst	G-band peak (cm^{-1})	Δ (cm^{-1})
N-G(900)	1591.21	+7.71
Co/N-G(900)	1598.92	
N-G(800)	1592.31	+4.41
Co/N-G(800)	1596.72	
N-G(700)	1594.52	+1.65
Co/N-G(700)	1596.17	
un-G	1595.07	+1.1
Co/un-G	1596.17	
B-G(700)	1595.62	-0.55
Co/B-G(700)	1595.07	
B-G(800)	1596.17	-3.31
Co/B-G(800)	1592.86	
B-G(900)	1596.72	-6.06
Co/B-G(900)	1590.66	

Table S5. Intensity ratio of the D-band and G-band (I_D/I_G) and specific activity of CO hydrogenation for N-G, un-G, and B-G at different annealing temperatures.

Catalyst	I_D/I_G	Specific activity ($mol_{CO}/mol_{Co}·s$)[a]
NG(900)	0.94	Not detected
NG(800)	0.87	Not detected
NG(700)	0.85	Not detected
un-G	0.81	Not detected
BG(700)	0.81	Not detected
BG(800)	0.86	Not detected
BG(900)	0.92	Not detected

[a] Reaction condition: 0.1 g of catalyst, [$CO/H_2/N_2/He$]=[7.3/14.6/7.3/70.8], 41 mL/min of total flow, 450 °C.

Defect level (or oxidation level) of graphene can be determined by the intensity ratio of D-band to G-band (I_D/I_G). In Raman spectra (Fig. S6), two peaks were observed; D-band (1344-1354 cm^{-1}) and G-band (1590-1599 cm^{-1}). G-band is graphitic peak related to sp^2 carbon atom vibration while D-band is disordered peak originated for defects and oxygen functionality.[S19-S21] As shown in Tables S5 and S6, I_D/I_G was increased according to annealing temperatures in both of catalysts with and without active metal (Co). In other word, defects of graphene were induced by high annealing temperature. To investigate the effect of defect level of graphene on catalytic activity of CO hydrogenation, we carried out reaction test with the catalyst without Co (Table S5). Activity was not detected even over N-G(900) and B-G(900) catalysts with high degree of defects. This indicates that defects have no direct influence on catalytic activity of CO hydrogenation unlike electrochemical reactions[S22-S24] (hydrogen evolution reaction; HER, and oxygen reduction reaction; ORR). In metal/graphene systems, it was revealed that defect can affect catalytic properties of metal, leading to variation in catalytic activity in ORR.[S25,S26] However, in this work, no dependence between catalytic activity and defect level was observed for CO hydrogenation reaction (Table S6 and Figure 2). It implies that effect of N or B doping on catalytic activity was dominant compared to that of defect level of graphene among Co/N-G, Co/un-G, and Co/B-G catalysts.

Table S6. Intensity ratio of the D-band and G-band (I_D/I_G) for Co/N-G, Co/un-G, and Co/B-G at different annealing temperatures.

Catalyst	I_D/I_G
Co/NG(900)	0.91
Co/NG(800)	0.81
Co/NG(700)	0.78
Co/un-G	0.77
Co/BG(700)	0.81
Co/BG(800)	0.84
Co/BG(900)	1.05

Table S7. Kinetic parameters for the CO hydrogenation over Co/N-G(900), Co/un-G, and Co/B-G(700), as calculated by the best fitted curve.

Catalyst	T (°C)	k_{app} ($mol_{CO} \cdot g_{cat}^{-1} \cdot min^{-1} \cdot atm^{-1}$)	K_{CO} (atm^{-1})
Co/N-G(900)	400°C	3.70×10^{-2}	3.27
	425°C	5.64×10^{-2}	1.99
	450°C	8.10×10^{-2}	1.53
Co/un-G	400°C	1.65×10^{-2}	6.27
	425°C	2.49×10^{-2}	5.97
	450°C	3.66×10^{-2}	5.52
Co/B-G(700)	400°C	1.51×10^{-2}	10.82
	425°C	2.16×10^{-2}	9.29
	450°C	3.33×10^{-2}	8.86

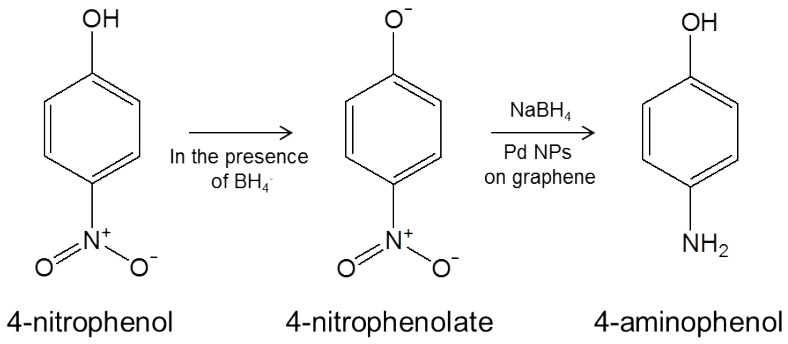

Scheme S1. Reaction scheme for the 4-nitrophenol reduction by $NaBH_4$.

References

S1. D. C. Marcano, D. V. Kosynkin, J. M. Berlin, A. Sinitskii, Z. Sun, A. Slesarev, L. B. Alemany, W. Lu, and J. M. Tour, *ACS Nano* 2010, **4**, 4806.

S2. R. Long, K. Mao, M. Gong, S. Zhou, J. Hu, M. Zhi, Y. You, S. Bai, J. Jiang, Q. Zhang, X. Wu, and Y. Xiong, *Angew. Chem. Int. Ed.* 2014, **53**, 3205.

S3. G. Kresse, and J. Furthmeller, *Phys. Rev. B* 1996, **54**, 11169.

S4. J. P. Perdew, K. Burke, and M. Ernzerhof, *Phys. Rev. Lett.* 1996, **77**, 3865-3868.

S5. P. E. Blöchl, *Phys. Rev. B* 1994, **50**, 17953.

S6. S. Grimme, *J. Comput. Chem.* 2006, **27**, 1787.

S7. R. F. W. Bader, Atoms in Molecules: A Quantum Theory, Oxford University Press, Oxford, **1990**.

S8. S. Jaliliab, and R. Vaziri, *Mol. Phys.* 2011, **109**, 687.

S9. T. Schiros, D. Nordlund, L. Pálová, D. Prezzi, L. Zhao, K. S. Kim, U. Wurstbauer, C. Gutiérrez, D. Delongchamp, C. Jaye, D. Fischer, H. Ogasawara, L. G. M. Pettersson, D. R. Reichman, P. Kim, M. S. Hybertsen, and A. N. Pasupathy, *Nano Lett.* 2012, **12**, 4025.

S10. J. Zhang, C. Zhao, N. Liu, H. Zhang, J. Liu, Y. Q. Fu, B. Guo, Z. Wang, S. Lei, and P. Hu, *Sci. Rep.* 2016, **6**, 28330.

S11. K. Okazaki-Maeda, T. Akita, S. Tanaka, and M. Kohyama, *Mater. Trans.* 2008, **49**, 2441.

S12. M. Ojeda, R. Nabar, A. U. Nilekar, A. Ishikawa, M. Mavrikakis, and E. Iglesia, *J. Catal.* 2010, **272**, 287.

S13. T. Sharifi, G. Hu, X. Jia, and T. Wågberg, *ACS Nano* 2012, **6**, 8904.

S14. M. Sahoo, K. P. Sreena, B. P. Vinayan, S. Ramaprabhu, *Mat. Res. Bull.* 2014, **61**, 383.

S15. F. Lin, and R. Doong, *Appl. Catal. A: Gen.* 2014, **486**, 32.

S16. S. mehmood, N. K. Janjua, F. Saira, and H. Fenniri, *J. Spectrosc.* 2016, doi:10.1155/2016/6210794.

S17. S. K. Ghosh, M. Mandal, S. Kundu, S. Nath, and T. Pal, *Appl. Catal. A: Gen.* 2004, **268**, 61.

S18. Z. D. Pozun, S. E. Rodenbusch, E. Keller, K. Tran, W. Tang, K. J. Stevenson, and G. Henkelman, *J. Phys. Chem. C* 2013, **117**, 7598.

S19. V. Gupta, N. Sharma, U. Singh, M. Arif, and A. Singh, *Optik* 2017, **143**, 115.

S20. A. A. Dubale, W.-N. Su, A. G, Tamirat, C.-J. Pan, B. A. Aragaw, H.-Ming Chen, C.-H. Chen, and B.-J. Hwang, *J. Mater. Chem. A* 2014, **2**, 18383.

S21. R. Wu, Y. Wang, L. Chen, L. Huang, and Y. Chen, *RSC Adv.* 2015, **5**, 49182.

S22. Y. Ito, W. Cong, T. Fujita, and M. Chen, *Angew. Chem. Int. Ed.* 2015, **54**, 2131.

S23. J. Zhang, and L. Dai, *ACS Catal.* 2015, 5, 7244.

S24. Y. Jia, L. Zhang, A. Du, G. Gao, J. Chen, X. Yan, C. L. Brown, and X. Yao, *Adv. Mater.* 2016, **28**, 9532.

S25. D. H. Lim, A. S. Negreira, and J. Wilcox, *J. Phys. Chem. C* 2011, **115**, 8961.

S26. D. H. Lim, and J. Wilcox, *J. Phys. Chem. C* 2011, **115**, 22742.